

Shape Resonances of the Transverse Magnetic Mode in a Spherically Stratified Medium

Umaporn Nuntaplook^{1,2*}, John A. Adam³

¹ Department of Mathematics, Faculty of Science, Mahidol University, Bangkok 10400, Thailand.

² Center of Excellence in Mathematics, Bangkok 10400, Thailand.

³ Department of Mathematics and Statistics, Old Dominion University, Norfolk, VA 23529, USA.

* Corresponding author. Tel.: +66 957596931; email: ununtaplook@gmail.com

Manuscript submitted November 24, 2017; accepted December 20, 2017.

doi: 10.17706/ijapm.2018.8.3.18-30

Abstract: Although morphology-dependent resonances (MDRs) have been studied for decades, it is interesting to note that TM resonances have not been as widely investigated as those of the TE mode. Nevertheless, the formers are also worthy of additional study. Even though the TE and TM mode resonances can be generated using the same technique, their properties (such as the additional sharp peak in the source function at the particle surface) are quite distinct. We present the derivation of the resonance formulations for TM mode for both increasing and decreasing piecewise-constant refractive index profiles in a two-layer model of a sphere embedded in a uniform medium of different refractive index. Numerical and graphical results are also provided.

Key words: Electromagnetic, resonance, transverse magnetic, stratified medium.

1. Introduction

In this paper we examine the shape resonance for the TM mode by a model of a piecewise constant refractive index in a two-layer spherical dielectric particle [1], [2] as shown in Fig. 1. The particle has its center at the origin of the coordinate system. The radius of the inner layer is a , and for the outer layer it is b . The refractive index in each region (and in the particle exterior) is assumed to be constant, where n_1 , n_2 , and n_3 are the refractive index in the inner, outer and exterior regions (1, 2 and 3 respectively). The refractive index n_3 in the exterior free space ($r > b$) is set equal to 1. The particle is assumed to be nonmagnetic and the complex time-dependence of the electric field is harmonic. The details of the resonance conditions for this model are developed in Section 2. The specific details for morphology-dependent resonances (MDRs) in this model are discussed in Section 3. The numerical calculations and graphical results for various refractive index profiles are presented in Section 4. The paper concludes with a discussion in Section 5.

2. Scattering Wave Theory

This section briefly discusses the standard theory of electromagnetic scattering from a spherical particle. As is well known from Maxwell's equations, for a spherically symmetric medium the electric E satisfies the following vector Helmholtz equation:

$$\nabla \times \nabla \times E - k^2 n^2(r)E = 0, \quad (1)$$

where k represents the free-space wave number and $n(r)$ represents the refractive-index profile.

It can be verified that the vector wave solutions of equation (1) can be computed by expanding the electric field in terms of the spherical vector wave functions for the transverse electric (TE) mode and the transverse magnetic (TM) modes [3].

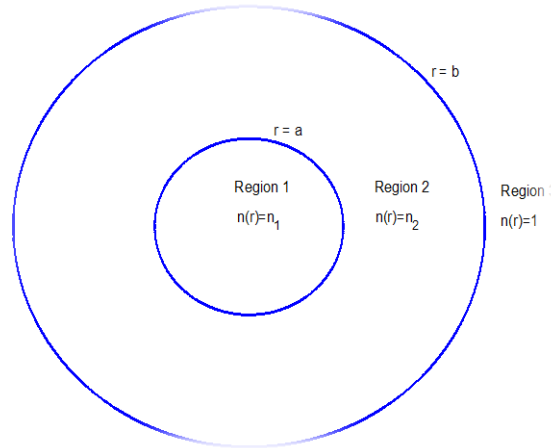


Fig. 1. A piecewise constant refractive index associated with a three-layer spherical dielectric particle.

To find the resonance conditions, it is necessary to focus on the radial Debye potentials $S_l(r)$ and $T_l(r)$, which satisfy the following second-order differential equations:

$$\frac{d^2 S_l(r)}{dr^2} + \left[k^2 n^2(r) - \frac{l(l+1)}{r^2} \right] S_l(r) = 0, \tag{2}$$

$$\frac{d^2 T_l(r)}{dr^2} - \frac{2}{n(r)} \frac{dn(r)}{dr} + \left[k^2 n^2(r) - \frac{l(l+1)}{r^2} \right] T_l(r) = 0 \tag{3}$$

where $S_l(r)$ is the radial Debye potential for the transverse electric (TE) fields, and the $T_l(r)$ is the corresponding potential for the transverse magnetic (TM) fields. Only equation (3) will only be discussed (TM mode) as the TE mode has been discussed elsewhere [4]. For the case of Mie scattering (when the refractive index has a constant value) the solutions $T_l(r)$ can be expressed in terms of the Riccati-Bessel functions [5], which are defined as

$$\psi_l(x) = x j_l(x), \tag{4}$$

$$\chi_l(x) = x y_l(x), \tag{5}$$

where $j_l(x)$ and $y_l(x)$ are spherical Bessel function of the first and second kinds, respectively. The solution is required to be finite at the origin, i.e. $T_l(0) = 0$. The solution of the internal region $0 \leq r \leq a$ is given by [1], [2]

$$T_l(r) = \psi_l(n_1 k r) \tag{6}$$

In regions 2 and 3 of the particle, the electric field consists of the incident wave and an outgoing scattered wave. The general solutions to (3) is linear combinations of the Riccati-Bessel functions. The solution in region 2, when $a < r \leq b$ is given by

$$T_l(r) = \bar{A}_l[\chi_l(n_2kr) + \bar{\psi}_l(n_2kr)], \quad (7)$$

and the external solution for $r \geq b$ is

$$T_l(r) = \bar{B}_l[\chi_l(kr) + \bar{\beta}_l\psi_l(kr)], \quad (8)$$

The constants $\bar{\alpha}_l$, $\bar{\beta}_l$, \bar{A}_l , and \bar{B}_l are determined by the condition that $T_l(r)$ and $T'_l(r)/n^2(r)$ be continuous for matching the internal and external solutions where the refractive index is discontinuous (such as at the surface of the sphere and at the boundaries between regions 1 and 2). These constants are derived as

$$\bar{A}_l = \frac{\psi_l(n_1x)}{\chi_l(n_2x) + \bar{\alpha}_l(n_2x)}, \quad (9)$$

$$\bar{B}_l = \frac{\bar{A}_l[\chi_l(n_2y) + \bar{\alpha}_l\psi_l(n_2y)]}{\chi_l(y) + \bar{\beta}_l\psi_l(y)}, \quad (10)$$

where

$$\bar{\alpha}_l = -\frac{(n_2\psi'_l(n_1x)\chi_l(n_2x) - n_1\psi_l(n_1x)\chi'_l(n_2x))}{(n_2\psi'_l(n_1x)\psi_l(n_2x) - n_1\psi_l(n_1x)\psi'_l(n_2x))} \quad (11)$$

$$\bar{\beta}_l = -(n_2\chi'_l(y)[\chi_l(n_2y) + \bar{\alpha}_l\psi_l(n_2y)] - \chi_l(y)[\chi'_l(n_2y) + \bar{\alpha}_l\psi'_l(n_2y)]) / (n_2\psi'_l(y)[\chi_l(n_2y) + \bar{\alpha}_l\psi_l(n_2y)] - \psi_l(y)[\chi'_l(n_2y) + \bar{\alpha}_l\psi'_l(n_2y)]), \quad (12)$$

where $x = ka$ and $y = kb$ are the size parameters.

3. Resonance Theory

The electromagnetic scattering problem has a direct connection to the quantum-mechanical problem. Electromagnetic energy can tunnel through the classically forbidden region and become temporarily trapped in resonance states. In the following section, we show the results of the case that the refractive index is a real quantity (though this is not necessary).

In Fig. (2) and (3) the shape of the potential well depends on the energy k^2 . These diagrams show the cases when the energy k^2 lies between the top and the bottom of the well. From (17) we see that when k increases, the bottom of the potential well will drop. The energy level k^2 will eventually coincide with the top of the well. In quantum mechanics, only certain levels of energy will satisfy the boundary conditions and are allowed in a potential well. The problem of shape resonance is similar in this regard. The radial Schrödinger equation in units such that $\hbar^2/2\mu = 1$, where $h = 2\pi\hbar$ is Planck's constant and μ is the reduced mass:

$$\frac{d^2\psi(r)}{dr^2} + \left[E - V(r) - \frac{l(l+1)}{r^2} \right] \psi(r) = 0, \quad (13)$$

where $V(r)$ is the potential energy function and E is the total energy of the system.

For the special case of a spherical particle with a piecewise constant refractive index, equation (3) and equation (13) will be identical if the potential function is defined as

$$V(r) = k^2[1 - n^2(r)]. \quad (14)$$

However, the *effective* potential is the sum of the potential function $V(r)$ and the centrifugal potential. It

is given by

$$V(r) = k^2[1 - n^2(r)] + \frac{l(l+1)}{r^2} \tag{15}$$

With

$$E = k^2. \tag{16}$$

Therefore, the potential in this problem is now defined as

$$V(r) = \begin{cases} k^2(1 - n_1^2) + l(l+1)/r^2, & 0 \leq r \leq a, \\ k^2(1 - n_2^2) + l(l+1)/r^2, & a \leq r \leq b, \\ l(l+1)/r^2, & r > b. \end{cases} \tag{17}$$

The nature of the potential (whether it is attractive, repulsive or some combination of the two) depends on the values of the refractive index and the wave number. For certain values of the energy level k^2 the wave particles will become temporally trapped inside the well, oscillating back and forth many times before finally exiting the classically forbidden region by tunnelling to the outside world. The name shape resonance comes from when the resonance behavior arises as a result of the potential shape i.e. whether it is the well or the barrier. Both increasing and decreasing refractive index profiles are considered.

For the case $n_1 < n_2$, the shape of the potential function is a single well as shown in Fig. 2. In case that n_2 is much larger than n_1 , the well will be deeper and wider. The classically allowed region is in $a_1 < r < R_2$. It is surrounded by the two forbidden regions $0 < r < a_1$ and $R_2 < r < b_1$. The point a_1 and b_1 are called the classical turning points. In the equivalent quantum-mechanical problem a particle can tunnel through the classically forbidden regions into the classically allowed potential well.

On the other hand, we have double wells for the case $n_1 > n_2$ as shown in Fig. 3. The most interesting feature of this case is that there are two classically allowed regions, $a_2 < r < R_1$ and $b_2 < r < R_2$. They are surrounded by the three classically forbidden regions $0 \leq r < a_2$, $R_1 < r < b_2$, and $R_2 < r < c_2$. The point a_2 , b_2 , and c_2 are called the classical turning points for this case. In the forbidden regions $r > b_1$ in Fig. 2 and $r < c_2$ in Fig. 3, the two functions $\psi_l(kr)$ and $\chi_l(kr)$ have opposite behaviors. When the function $\psi_l(kr)$ has exponential-like increasing rapidly in this region, the function $\chi_l(kr)$ has exponential-like decreasing behavior.

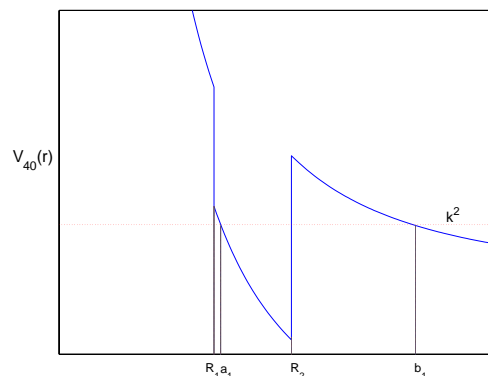


Fig. 2. A potential for increasing refractive index profile.

The resonance will occur in the classically allowed regions, then the wave function will continue decay monotonically in the barrier regions to ensure that it vanishes when $r \rightarrow \infty$.

Based on the behavior of the Ricatti-Bessel functions, the behavior of the function $\psi_l(kr)$ is increasing

monotonically, but $\chi_l(kr)$ has the opposite behavior. Therefore, we need only the function $\chi_l(kr)$ in the barrier region. The necessary conditions for to determine the location of the resonances are $\bar{\alpha}_l = 0$ and $\bar{\beta}_l = 0$.

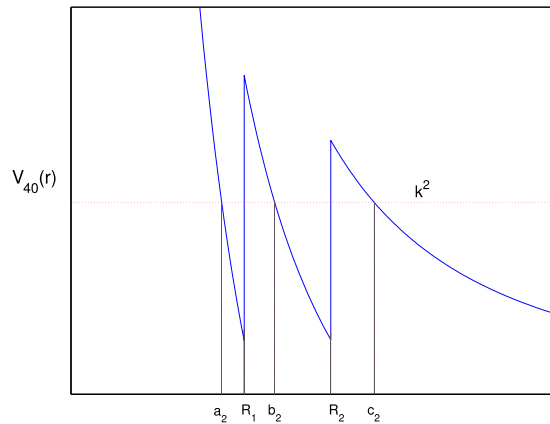


Fig. 3. A potential for decreasing refractive index profile.

4. Numerical Results

By solving for the size parameters x and y from the conditions $\bar{\alpha}_l = 0$ and $\bar{\beta}_l = 0$, there are infinitely many discrete values that satisfy the conditions. However, there are only finite values are in the range between the top and the bottom of the potential well. The solutions above the top and below the bottom of the well are not classified as resonances because they are too wide to have the properties discussed above.

For specific values of the energy level, the particles will become temporally trapped in the well, oscillating back and forth many times and finally tunnelling back through the classical forbidden region to the outside world. This is where we found the shape resonances of this three-layer model. In this section, we show the numerical results of five cases 1-5. The results show the radial wave functions for increasing refractive index profiles: $n_1 = 1.2$, $n_2 = 1.5$, with $l = 40$ (Case 1) and with $l = 53$ (Case 5) ; $n_1 = 1.33$, $n_2 = 1.47$, with $l = 53$ (Case 3), and for decreasing refractive index profiles $n_1 = 1.5$, $n_2 = 1.2$, with $l = 40$ (Case 2); $n_1 = 1.47$, $n_2 = 1.33$, with $l = 53$ (Case 4) with $l = 40$ (Case 5).

CASE 1: Radial wave functions for increasing refractive index profile when $n_1 = 1.2$, $n_2 = 1.5$, and $l = 40$.

Fig. 4 shows the wave function $T_{40}(r)$ along with the potential function $V_{40}(r)$ for $n_1 = 1.2$, $n_2 = 1.5$, and $l = 40$. This potential supports three TM resonances for specific values of x . They are located at $x = 30.02853$ with $y = 32.73812$ (a), $y = 35.83863$ (b), and $y = 38.58294$ (c).

Fig. 5 shows the change pattern that the wave function experiences as the system transverse the TM for the case of $n_1 < n_2$ with $n_1 = 1.2$, $n_2 = 1.5$, and $l = 40$. The panel (a) shows the case that $x = 30.02853$ and $y = 32.93812$ which is above the resonance. The panel (b) shows the wave function for case $x = 30.02853$ and $y = 32.73812$, which is the resonance case. The panel (c) shows the wave functions for the case $x = 30.02853$ and $y = 32.53812$ which is below the resonance.

Fig. 6 shows the wave function $T_{40}(r)$ along with the potential function $V_{40}(r)$ for $n_1 = 1.2$, $n_2 = 1.5$, and $l = 40$. This potential supports three TM resonances for specific values of x . They are located at $x = 34.63927$ with $y = 35.83863$ (a), and $y = 38.58294$ (b).

CASE 2: Radial wave functions for decreasing refractive index profile when $n_1 = 1.5$, $n_2 = 1.2$, and $l = 40$.

Fig. 7 shows the wave function $T_{40}(r)$ along with the potential function $V_{40}(r)$ for $n_1 = 1.5$, $n_2 = 1.2$, and $l = 40$. This potential supports three TM resonances. They are located at $x = 30.36620$, $y = 35.18550$ (a); $x = 33.88184$, $y = 35.18550$ (b); $x = 33.88184$, $y = 40.01353$ (c).

Fig. 8 shows the change of pattern that the wave function experiences as the system transverses the TM for the case of $n_1 > n_2$ with $n_1 = 1.5$, $n_2 = 1.2$, and $l = 40$. For the specific value of for $y = 35.18550$, x -value slightly above resonance $x = 30.96620$ (a); on resonance $x = 30.36620$ (b); below resonance $x = 30.06620$ (c).

Fig. 9 shows the change of pattern that the wave function experiences as the system transverses the TM for the case of $n_1 > n_2$ with $n_1 = 1.5$, $n_2 = 1.2$, and $l = 40$. For the specific value of for $x = 30.36620$, y -value slightly above resonance $y = 35.98550$ (a); on resonance $y = 35.18550$ (b); below resonance $y = 34.18550$ (c).

CASE 3: Radial wave functions for increasing refractive index profile when $n_1 = 1.33$, $n_2 = 1.47$, and $l = 53$.

Fig. 10 shows the wave function $T_{53}(r)$ along with the potential function $V_{53}(r)$ for $n_1 = 1.33$, $n_2 = 1.47$, and $l = 53$. This potential supports three TM resonances for specific values of x . They are located at $x = 40.51258$, $y = 42.81402$ (a); $y = 46.27614$ (b); $y = 49.29485$ (c); $y = 52.14311$ (d).

Fig. 11 shows the change of pattern that the wave function experiences as the system transverses the TM for the case of $n_1 < n_2$ with $n_1 = 1.33$, $n_2 = 1.47$, and $l = 53$. For the specific value of for $x = 40.51258$, y -value slightly above resonance $y = 42.91402$ (a); on resonance $y = 42.81402$ (b); below resonance $y = 42.71402$ (c).

CASE 4: Radial wave functions for decreasing refractive index profile when $n_1 = 1.47$, $n_2 = 1.33$, and $l = 53$.

Fig. 12 shows the wave function $T_{53}(r)$ along with the potential function $V_{53}(r)$ for $n_1 = 1.47$, $n_2 = 1.33$, and $l = 53$. This potential supports three TM resonances for specific values of x . They are located at $x = 39.60994$, $y = 42.18343$ (a); $y = 47.00389$ (b); $y = 50.66246$ (c); $y = 54.40982$ (d).

Fig. 13 shows the change pattern that the wave function experiences as the system transverses the TM for the case of $n_1 > n_2$ with $n_1 = 1.47$, $n_2 = 1.33$, and $l = 53$. For the specific value of for $x = 39.60994$, y -value slightly above resonance $y = 47.90389$ (a); on resonance $y = 47.00389$ (b); below resonance $y = 46.00389$ (c).

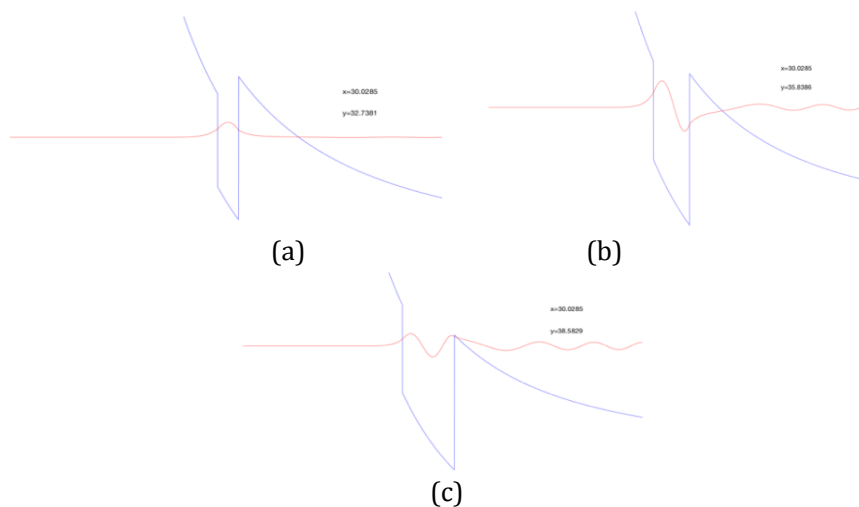


Fig. 4. Radial wave functions for three TM resonances with $x = 30.02853$, $y = 32.73812$ (a); $x = 30.02853$, $y = 35.83863$ (b); $x = 30.02853$, $y = 38.58294$ (c), corresponding to the refractive index profile $n_1 = 1.2$, $n_2 = 1.5$, and $l = 40$.

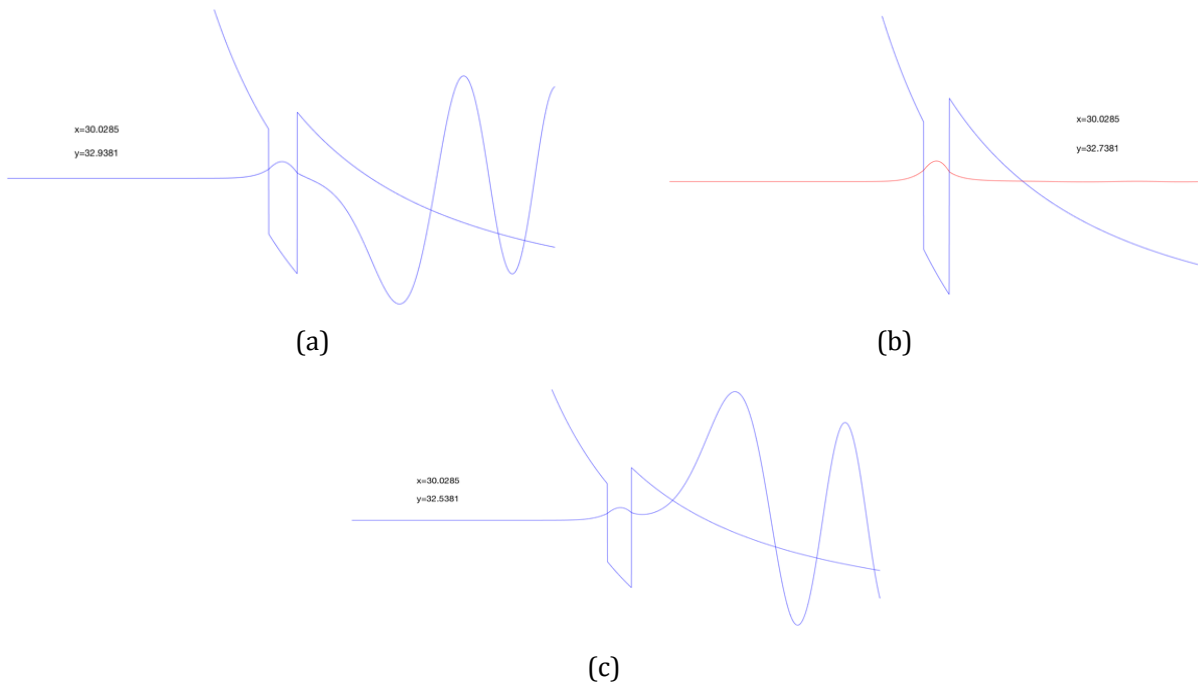


Fig. 5. Behavior of the TM wave function in the vicinity of a resonance for the case $n_1 = 1.2$, $n_2 = 1.5$, and $l = 40$; for $x = 30.02853$, the behavior for a size parameter y -value slightly above resonance $y = 32.93812$ (a); on resonance $y = 32.73812$ (b); below resonance $y = 32.53812$ (c).

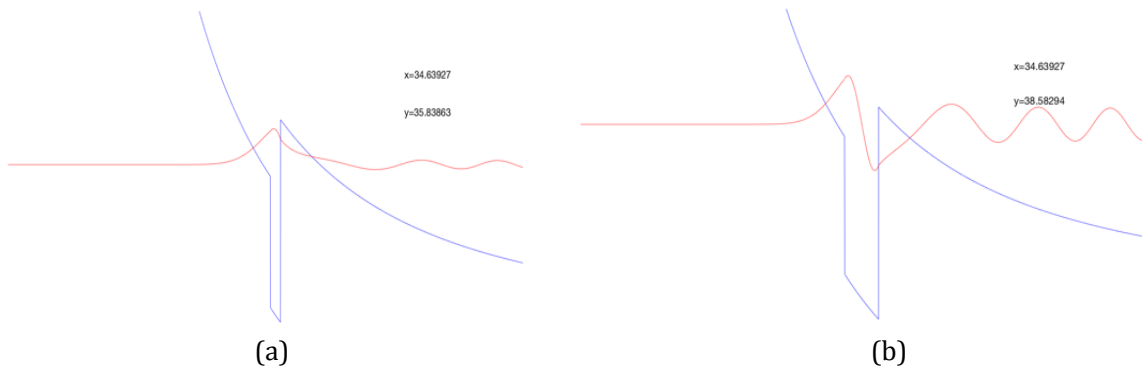
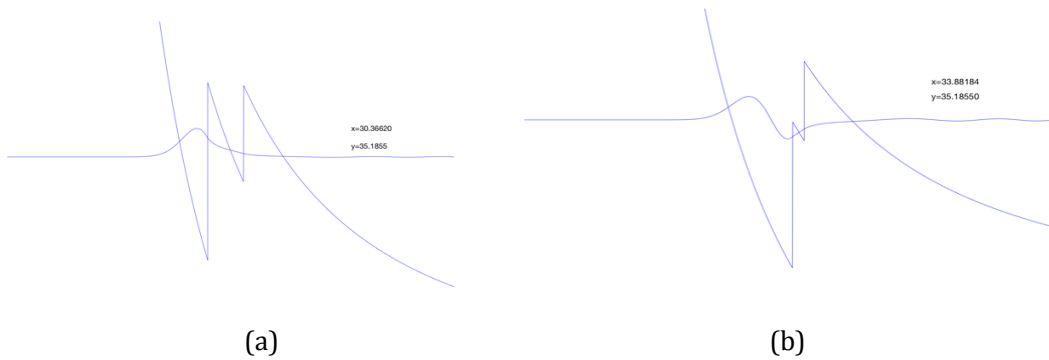
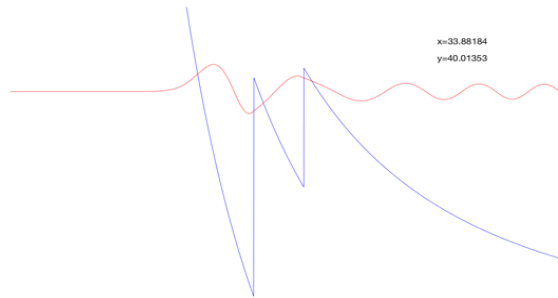


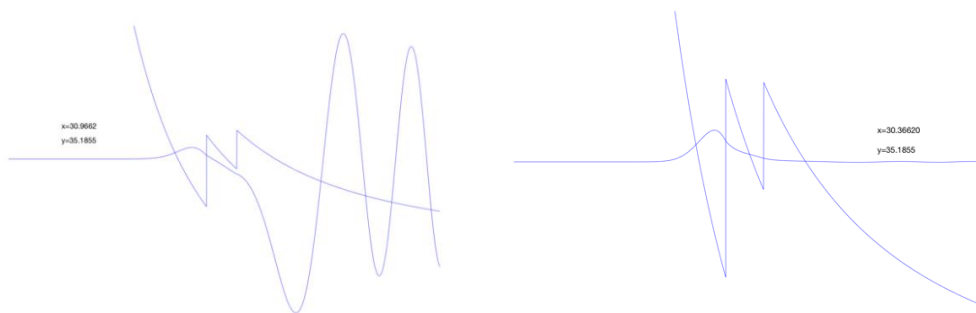
Fig. 6. Radial wave functions for two TM resonances with $x = 34.63927$, $y = 35.83863$ (a); $x = 34.63927$, $y = 38.58294$ (b), corresponding to the refractive index profile $n_1 = 1.2$, $n_2 = 1.5$, and $l = 40$.





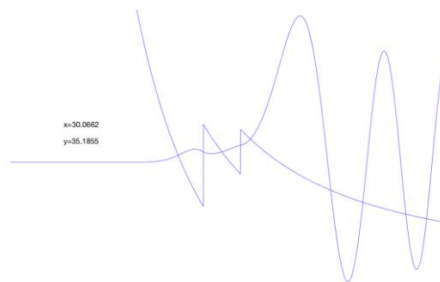
(c)

Fig. 7. Radial wave functions for three TM resonances with $x = 30.36620$, $y = 35.18550$ (a); $x = 33.88184$, $y = 35.18550$ (b); $x = 33.88184$, $y = 40.01353$ (c), corresponding to the refractive index profile $n_1 = 1.5$, $n_2 = 1.2$, and $l = 40$.



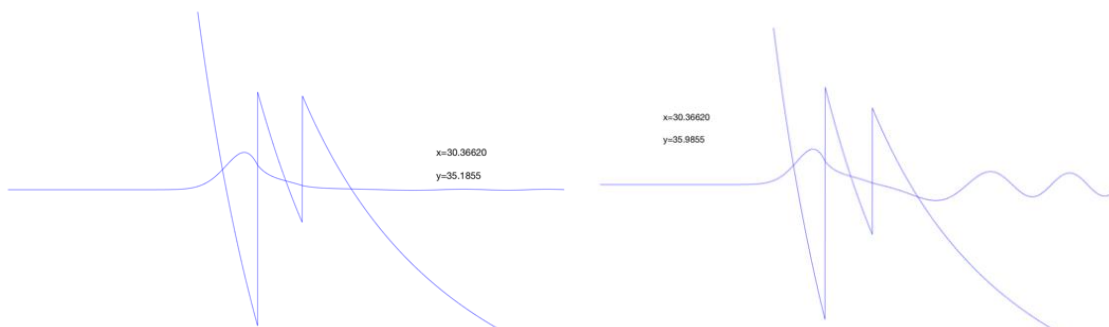
(a)

(b)



(c)

Fig. 8. Behavior of the TM wave function in the vicinity of a resonance for the case $n_1 = 1.5$, $n_2 = 1.2$, and $l = 40$; for $y = 35.18850$, the behavior for a size parameter x -value slightly above resonance $x = 30.96620$ (a); on resonance $x = 30.36620$ (b); below resonance $x = 30.06620$ (c).



(a)

(b)

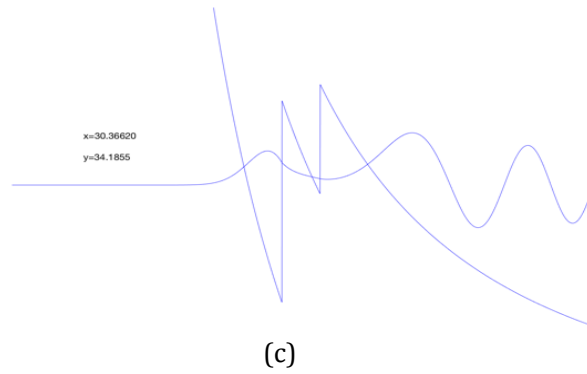


Fig. 9. Behavior of the TM wave function in the vicinity of a resonance for the case $n_1 = 1.5$, $n_2 = 1.2$, and $l = 40$; for $x = 30.36620$, the behavior for a size parameter y -value slightly above resonance $y = 35.98850$ (a); on resonance $y = 35.18850$ (b); below resonance $y = 34.18850$ (c).

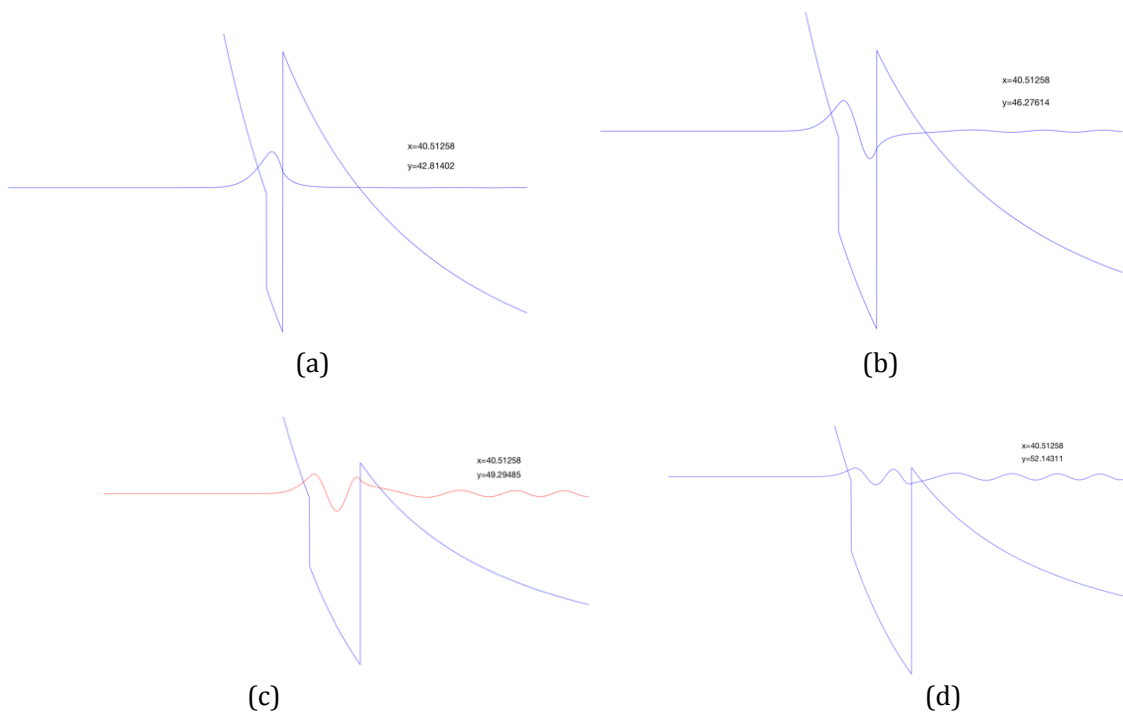
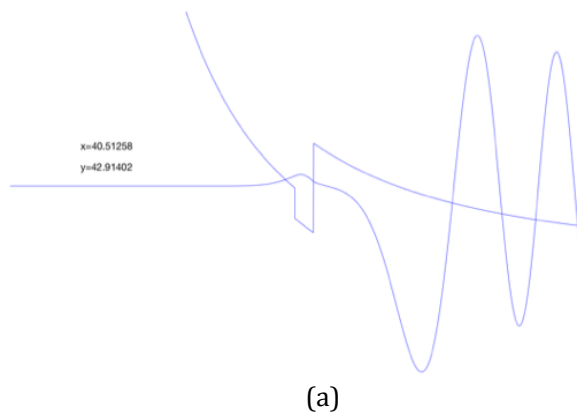


Fig. 10. Radial wave functions for three TM resonances with $x = 40.51258$, $y = 42.81402$ (a); $x = 40.51258$, $y = 46.27614$ (b); $x = 40.51258$, $y = 49.29485$ (c), $x = 40.51258$, $y = 52.14311$ (d), corresponding to the refractive index profile $n_1 = 1.33$, $n_2 = 1.47$, and $l = 53$.



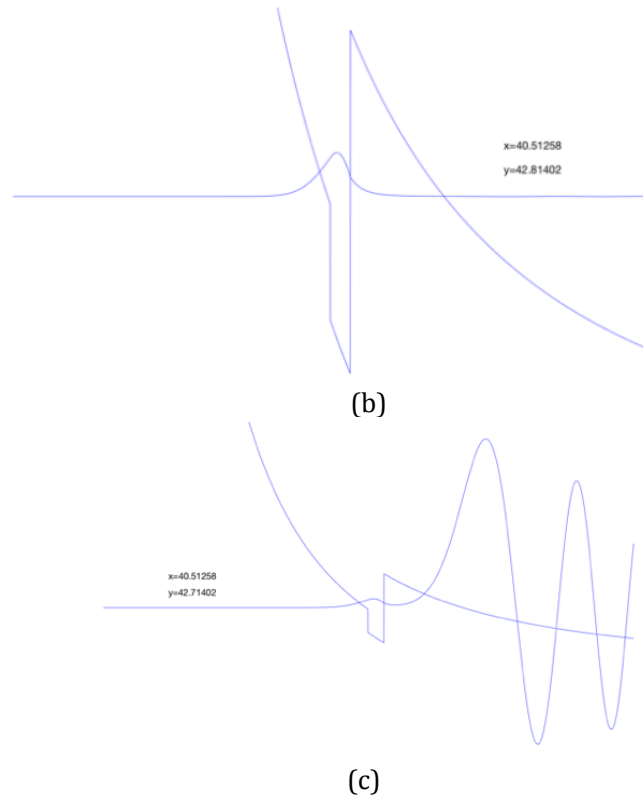


Fig. 11. Behavior of the TM wave function in the vicinity of a resonance for the case $n_1 = 1.33$, $n_2 = 1.47$, and $l = 53$; for $x = 40.51258$, the behavior for a size parameter y -value slightly above resonance $y = 42.91402$ (a); on resonance $y = 42.81402$ (b); below resonance $y = 42.71402$ (c).

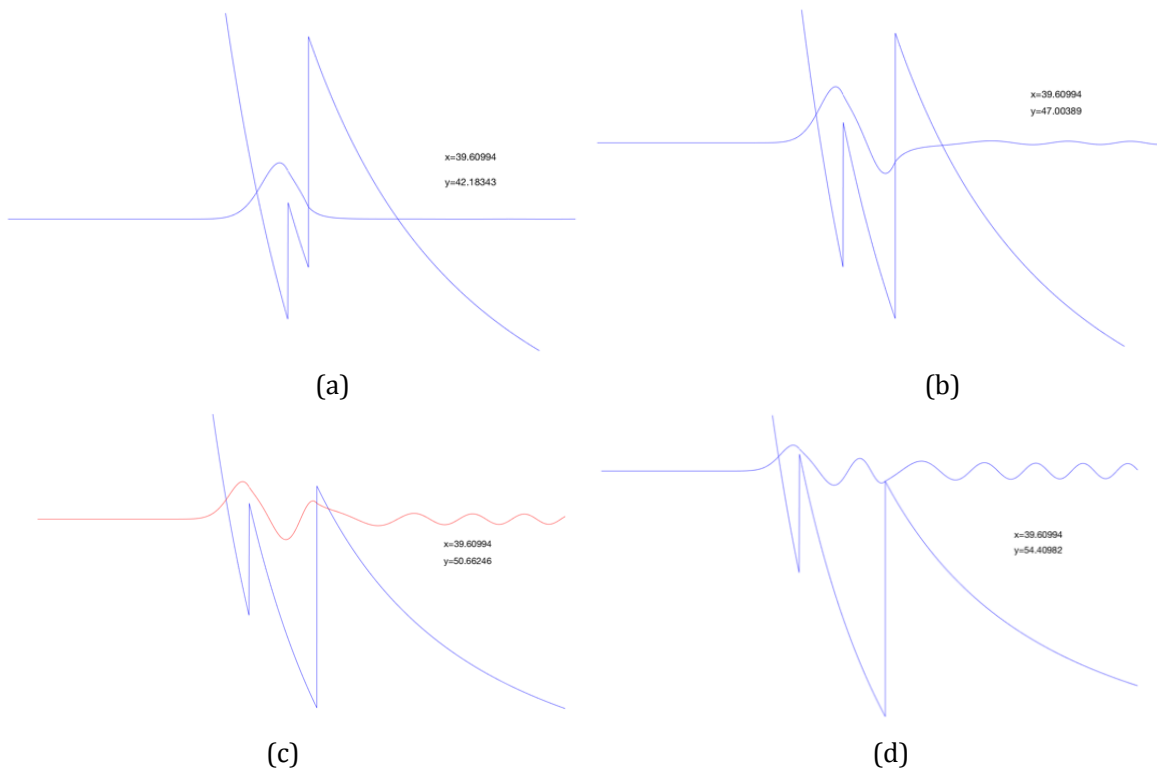


Fig. 12. Radial wave functions for three TM resonances with $x = 39.60994$, $y = 42.18343$ (a); $x = 39.60994$, $y = 47.00389$ (b); $x = 39.60994$, $y = 50.66246$ (c); $x = 39.60994$, $y = 54.40982$ (d), corresponding to the refractive index profile $n_1 = 1.47$, $n_2 = 1.33$, and $l = 53$.

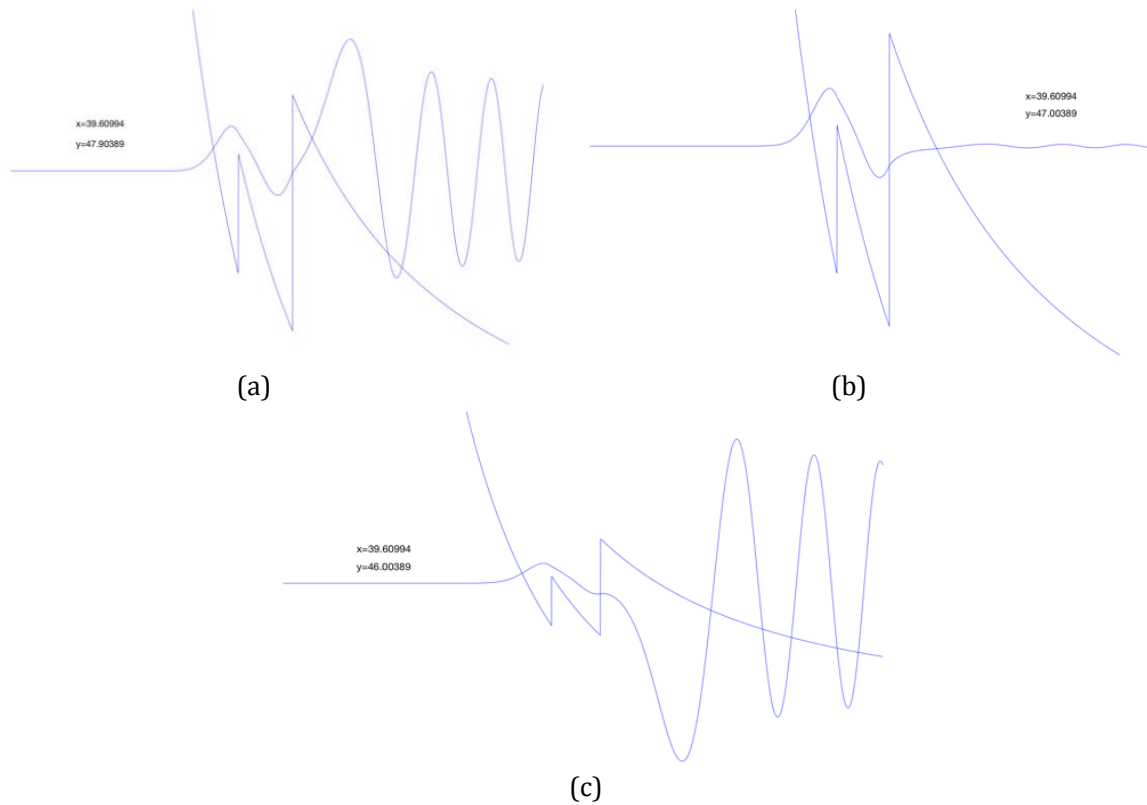


Fig. 13. Behavior of the TM wave function in the vicinity of a resonance for the case $n_1 = 1.47$, $n_2 = 1.33$, and $l = 53$; for $x = 39.60994$, the behavior for a size parameter y -value slightly above resonance $y = 47.90389$ (a); on resonance $y = 47.00389$ (b); below resonance $y = 46.00389$ (c).

CASE 5: Special case for radial wave functions for decreasing refractive index profile when $n_1 = 1.2$, $n_2 = 1.5$, and $l = 53$; and when $n_1 = 1.47$, $n_2 = 1.33$, and $l = 40$.

Fig. 14 shows the wave function $T_{53}(r)$ along with the potential function $V_{53}(r)$ for $n_1 = 1.2$, $n_2 = 1.5$, and $l = 53$. This potential supports three TM resonances for specific values of x . They are located at $x = 38.87206$, $y = 41.99603$.

Fig. 15 shows the wave function $T_{40}(r)$ along with the potential function $V_{40}(r)$ for $n_1 = 1.47$, $n_2 = 1.33$, and $l = 40$. This potential supports three TM resonances for specific values of x . They are located at $x = 30.64486$, $y = 32.15745$ (a); $y = 36.48708$ (b).

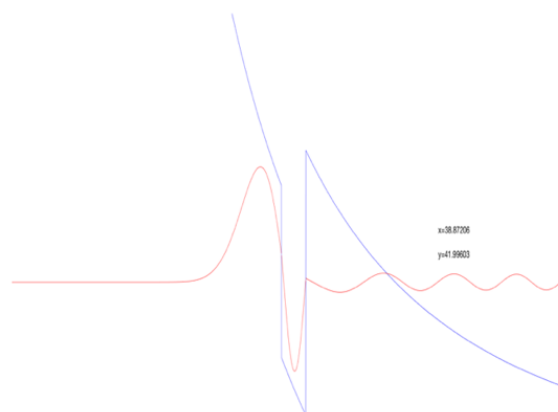


Fig. 14. Radial wave functions for three TM resonances with $x = 38.87206$, $y = 41.99603$ corresponding to the refractive index profile $n_1 = 1.2$, $n_2 = 1.5$, and $l = 53$.

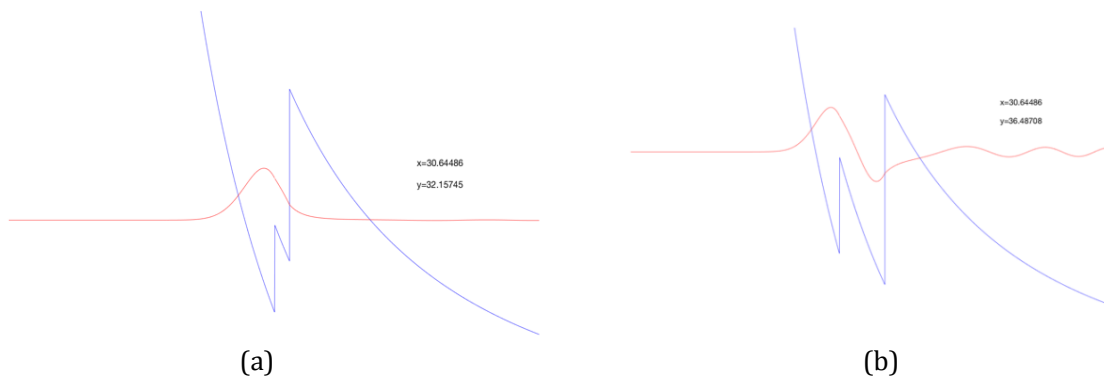


Fig. 15. Radial wave functions for three TM resonances with $x = 30.64486$, $y = 32.15745$ (a); $x = 30.64486$, $y = 36.48708$ (b), corresponding to the refractive index profile $n_1 = 1.47$, $n_2 = 1.33$, and $l = 40$.

5. Discussion

Obviously, the most interesting feature of the resonance happens in the classically allowed region $a_1 < r < R_2$ for the case of increasing refractive index, and in the regions $a_2 < r < R_1$ and $b_2 < r < R_2$ for the case of decreasing refractive index. If we reduce the layer of the model to a single layer sphere, the numerical results for the case of refractive index $n_1 = 1.47$ and $l = 40$ are satisfied with the results by [1], and the case that $n_1 = 1.47$ and $l = 53$ is agreed with the results by [6].

Moreover, the lowest-level wave function has a single peak, and the higher levels will have more peaks alternating between positive and negative energy levels. Figures 5, 8, 9, 11, and 13 demonstrate the change patterns that the wave function transverses the TM for both increasing and decreasing refractive indices. The wave functions $T_{40}(r)$ and $T_{53}(r)$ for the case that the value of x or y is above the resonance show an exponential-like increase in the tunnelling region. The amplitude of the wave function outside the particle $r > R_2$ is much larger than the amplitude inside the particle. The case that the value of x and y are on the resonance shows the wave function has an exponential-like decrease in the tunnelling region. The amplitude of the wave function inside the particle is much larger than the amplitude outside because the field strength increases rapidly in the layer just outside the surface, $R_2 < r < b_1$ for the case $R_2 < r < c_2$ and then continues to a maximum inside the particle near the surface (both inside and outside). This is sufficient to define a resonance. The case that the value of x or y is below the resonance shows that the wave function has an increase exponential-like manner in the tunnelling region. This case is very similar to the case that the value of x or y is above the resonance except that the exponential-like growth in the tunnelling region is in the negative direction, i.e., opposite to the above resonance case.

Comparing the radial wave functions between Case 1 when $n_1 = 1.2$, $n_2 = 1.5$, and $l = 40$ (shown in Fig. 4 and 6) and Case 5 when $n_1 = 1.2$, $n_2 = 1.5$, and $l = 53$ (shown in Figure 14); and Case 4 when $n_1 = 1.47$, $n_2 = 1.33$, and $l = 53$ (shown in Figure 12) and Case 5 when $n_1 = 1.47$, $n_2 = 1.33$, and $l = 40$ (shown in Figure 15), it is simply shown that the resonance values of x and y vary as the value of the angular momentum l .

References

- [1] Johnson, B. R. (1993). Theory of morphology-dependent resonances: Shape resonances and width formulas. *Journal of the Optical Society of America A*, 10, 343-352.
- [2] Johnson, B. R. (1999). Exact theory of electromagnetic scattering by a heterogeneous multilayer sphere in the infinite-layer limit: effective-media approach. *Journal of the Optical Society of America A*, 16,

845-852.

- [3] Wyatt, P. J. (1962). Scattering of electromagnetic plane waves from inhomogeneous spherically symmetric objects. *Physical Review*, 127(5), 1837-1843.
- [4] Westcott, B. S. (1968). Exact solutions for electromagnetic wave propagation in spherically stratified isotropic media. *Proc. Camb. Phil. Soc*, 64, 227-235.
- [5] Abramowitz, M., & Stegun, I. A. (1965). *Handbook of Mathematical Functions with Formulas, Graphs, and Mathematical Tables*. Dover Publications, Inc., New York.
- [6] Chylek, P., Pendleton, J. D., & Pinnick, R. G. (1985). Internal and near-surface scattered field of a spherical particle at resonant conditions. *Journal of Applied Optics*, 24(23), 3940-3942.



Umaporn Nuntaplook received her Ph.D. in computational and applied mathematics from Old Dominion University, USA, in 2013. Currently she is a lecturer at the Department of Mathematics, Mahidol University, Bangkok, Thailand. Her research interests are applying the computational methods to the problems in the fields of mathematical physics including the topics in electromagnetic, acoustic, and potential scattering theory.



John A. Adam is professor of mathematics at the Department of Computational and Applied Mathematics (Old Dominion University, USA) and have had varied research interests, from astrophysical MHD and the related singular differential equations, to modeling tumor growth and wound healing. His current area of research is in theoretical meteorological optics, specially ray and wave propagation in radially inhomogeneous media, with potential applications to the study of certain types of metamaterials. He has

written several books published by Princeton University Press.